Received: 30 September 2022 | Revised: 3 March 2023 | Accepted: 21 March 2023

DOI: 10.1002/eqe.3886

RESEARCH ARTICLE

WILEY

The effect of vertical motions on damage accumulation on concrete gravity dams

Berat Feyza Soysal[1] | **Yalin Arici**[2] | **Bekir Özer Ay**[3]

[1]Department of Civil Engineering, Cankaya University, Ankara, Turkey

[2]Department of Civil Engineering, Middle East Technical University, Ankara, Turkey

[3]Department of Architecture, Middle East Technical University, Ankara, Turkey

Correspondence
Berat Feyza Soysal, Department of Civil Engineering, Cankaya University, Ankara, Turkey.
Email: fsoysal@cankaya.edu.tr

Abstract

The effect of vertical ground motions on the seismic response of dams has long been a concern in the seismic design and evaluation of concrete gravity dams. The guidelines regarding the use of vertical motions in time history analysis (THA) are not clear due to the complexity of the effect as well as the large uncertainty in the motion selection process. The goal of this study is to assess the significance of vertical motions' effects on concrete gravity dams considering the relevant variability due to ground motion, system frequency response as well as the shaking level. To this end, a carefully selected ground motion set providing realistic vertical(V)/horizontal(H) loading was used in nonlinear THAs of three different systems with different modal properties. In order to evaluate the intensity of shaking on the vertical motions' effect, the responses were calculated at different seismic levels corresponding to operation, design, and maximum shaking levels. Along with traditional demand parameters commonly employed in assessing seismic response, cracking on the base and at the upstream face of the monolith was adopted as demand measures using a model capable of yielding discrete cracking on the system. The effect of vertical motions was quantified by comparing the response of $H + V$ to H only shaking. The results show the vertical shaking can significantly affect upstream cracking for the operation or design level earthquakes, the effect increasing for larger dams.

KEYWORDS

discrete crack, gravity dam, modified applied element method, motion selection, seismic response, vertical motion

1 | INTRODUCTION

Concrete gravity dams form a very important part of power generation and water supply infrastructure. The design and analysis of these structures are now being conducted using nonlinear analysis methods with time history analyses (THAs). A complex part of the uncertainty regarding the ground motions is the three-dimensional (3D) nature of the motion with increasing concern on the effect of vertical shaking on infrastructure. The effect of vertical motions has generally not been considered in the analysis of concrete gravity dams pertaining to the early suggestions of small effect on the stress response. The uncertainty in this field is also due to the use of different demand parameters in different studies with the

NOVELTY

- The effect of vertical accelerations on gravity dams assessed focusing on damage.
- Motion variability included using a large set complying with site V/H suggestions.
- The vertical motions' effect quantified for different shaking levels and systems.
- The vertical motions' effect increased with increasing system size and period.
- The effect reduced with increasing shaking level at the site.

varying effect of the vertical motion on the chosen response quantity. Correspondingly, the use of vertical shaking in the seismic analysis of concrete gravity dams and corresponding effects is a gray area in the analysis due to the uncertainty inherent in ground motions, the one of a kind nature of dam systems as well as the varying effects on vertical shaking on different demand parameters.

The concerns about the effects of vertical shaking (V) have been present since the undertaking of rigorous modeling on the seismic response of dam systems. Initial work focused on the robust modeling of complex soil–structure–reservoir interaction concluded the effect of vertical acceleration on the induced stresses and displacements was not critical.[1] With the increase in the computational power, nonlinear THA were increasingly viable for the seismic assessment of gravity dams. The first comprehensive coverage regarding the effect of ground motions using nonlinear THA, as presented in Léger and Leclerc,[2] agreed with the former conclusions for nonlinear response. The inclusion of vertical acceleration component along with the horizontal (H), that is, $H + V$ analysis, was concluded to not change the critical scaling factor defined as the peak ground acceleration (PGA) level for the horizontal ground motion of a THA. A recent study by Hariri-Ardebili and Saouma[3] suggests otherwise considering vertical motion's effect on crest displacement. The conclusion in Hariri-Ardebili et al.[4] is less clear on the difference of using vertical motions evaluating the crack pattern on the Koyna Dam while confirming negligible effect in linear elastic range in accordance with the earlier studies by Chopra. Comparing the effects of vertical motion component for 20 motions, very mild increases in displacement, dissipated energy and local damage indices were presented in Wang et al.[5] As given above, while the initial conclusions on insignificance of the effect of vertical motions are contradicted in later work, a quantification of the effect is not clearly available.

The principal stresses or crest displacements are two conventional demand parameters utilized for quantifying the behavior of concrete gravity dams as well as assessing the effect of vertical shaking. While these are practically obtained from simulations, the correlation to damage is not clear. In the nonlinear range, damage on these systems has been quantified using dissipated energy and corresponding model dependent local damage indices from the finite element analyses. On the other hand, the damage on concrete gravity dams can be defined in terms of the major concern which is the cracking on the system. This requires an approach capable of simulating the discrete nature of cracking in brittle media allowing discontinuities in the computational domain. One such approach, the Applied Element Method (AEM), is used in this study. The AEM, compared to counterparts like the computationally very costly distinct element method, DEM,[6] allows modeling of large size systems with the inclusion of discrete cracking. An improved AEM formulation, the Modified Applied Element Method (MAEM), including the Poisson effect and tensile softening response was presented in Soysal Albostan[7] for the simulation of the response of dam monoliths. The model can show discrete crack opening, the primary form of damage on these systems, as well as yielding conventional demand parameters, enabling a general assessment of the effect of vertical shaking on the response.

In the context of the discussion above, the primary goal of this study is to quantify the effect of the vertical motion on concrete gravity dams using upstream (U/S) cracking as the primary damage measure. The Modified Applied Element approach was used to this end. In order to include the variability of system geometry (i.e., modal frequencies), three different typical sections were evaluated with the chosen motion sets. The uncertainty in the ground motions was tackled by proper selection and amplitude scaling of motions for monoliths for site-specific uniform hazard spectra (UHS). The effect of the level of shaking was considered using different target levels, loosely corresponding to common design levels, that is, operation-based earthquake (OBE), maximum design earthquake (MDE), and maximum credible earthquake (MCE). For different shaking levels and systems, the effect of vertical motions was quantified in terms of a number of engineering demand parameters (EDPs) such as the crest response and the post-seismic factor of safety values along with the cracking on the U/S face. The response from the analysis without (H only) and with ($H + V$) vertical ground motions were compared, and the differences were quantified in an average sense. The effect of the vertical motion on the response for different choice of target spectra, that is, using average hazard and vertical target spectrum, was also evaluated.

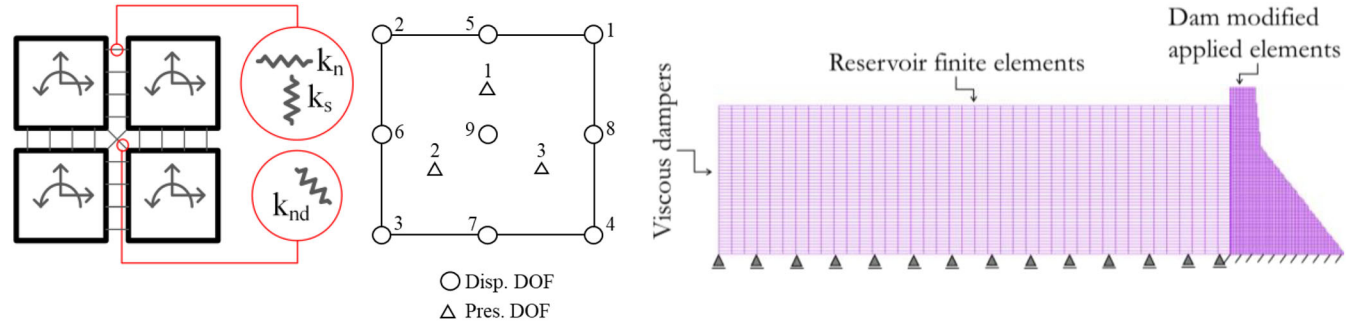

(A) Modified applied element method (B) Reservoir finite element (C) Dam – reservoir modeling

FIGURE 1 Modified applied element method.

This study is arranged as follows. First, the formulation for the modified applied element model and the relevant validation studies are presented in a concise fashion. After the presentation of the utilized generic dam models, the selection study for the utilized ground motion pairs is discussed. The results of the simulations for the three chosen dam systems are presented next: at three different earthquake levels, the response of the systems are compared with and without the use of vertical ground motions. The effect of vertical motions on different demand parameters including crack width is quantified in a statistical fashion. Conclusions of the study are presented at the very end of the paper.

2 | DAM AND RESERVOIR MODELING

The dam-reservoir system (Figure 1C) is discretized using modified applied elements (Figure 1A) and mixed pressure-displacement fluid elements (Figure 1B), respectively. The modified applied element formulation includes diagonal springs (135°/45° with respect to horizontal) as well as normal and shear springs between the elements. The elements enable the representation of the Poisson effect for accurate modeling of the elastic states of stress. The systems were assumed to be seated on rigid foundation rock. The effect of vertical ground motions are larger for the rigid foundation case (Fenves and Chopra[8]), indicating the results provided should be considered as an upper bound for other foundation conditions.

2.1 | Theory and formulation in elastic range

The forces at the degrees of freedom can be obtained directly from spring deformations in the AEM leading to a simple setup of equilibrium equations. The formation of the element stiffness matrix depending on spring pairs' coordinates around the rigid body is presented in Meguro and Tagel-Din.[9] The update of the global stiffness matrix for a diagonal connection with a spring stiffness of k_{nd} is presented in detail in Soysal Albostan.[7] The updated formulation allows the modeling of the Poisson effect. Unlike other discrete element or rigid body-spring models, different Poisson ratios can be represented in the system.

The simulation of a continuum using a lattice-like spring/rigid body system requires determining the elastic constants of the model (the spring constants) corresponding to the proper representation of strain energy distribution in the system for the two-dimensional (2D) plane stress condition. The relationship between macromaterial constants such as Young's modulus, E, and Poisson's ratio, υ, and the microspring parameters k_n, k_s, and k_{nd}, which are the spring stiffness constants for normal, shear, and diagonal springs, respectively, are calculated based on the Cauchy–Born rule and hyper-elastic theory using the concept of strain energy in Soysal Albostan[7] (Equation 1). In these equations, s and t correspond to the number of spring pairs between the elements and the thickness of the element, respectively.

$$k_n = \frac{Et}{(1+\nu)s} \quad k_s = \frac{Et(1-3\nu)}{(1-\nu^2)s} \quad k_{nd} = \frac{Et\nu}{(1-\nu^2)} \tag{1}$$

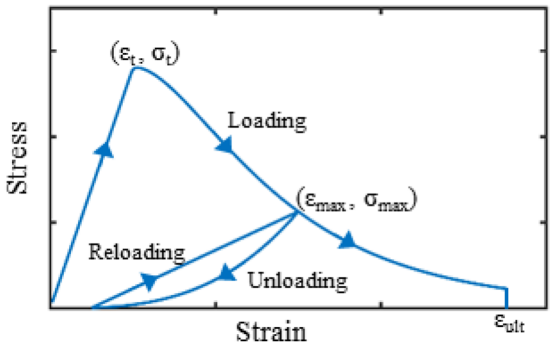

FIGURE 2 Tensile behavior.

2.2 | Tensile softening and fracture energy for nonlinear response

The modeling of tension softening in concrete is required to obtain a realistic model response for concrete structures. Tension softening (Figure 2) is implemented for the horizontal and vertical normal springs: A linear elastic response is assumed until the cracking point (ε_t,σ_t); upon the exceedance of this limit, the loading curve has an exponential form proposed by Lubliner et al.[10]: $\sigma = \sigma_t\,(2\exp(-b(\varepsilon-\varepsilon_t)) - \exp(-2b(\varepsilon-\varepsilon_t)))$ defined by the parameter b. The unloading-reloading response around the past maximum strain (ε_{max},σ_{max}) is based on Maekawa et al.[11] The diagonal springs are brittle upon the exceedance of tensile strain, ε_t. When the normal spring pair reaches the softening branch, shear springs can no longer carry force or contribute to the stiffness of the system.

The fracture energy in discrete cracks is intrinsic in this model and directly proportional to the length of the crack. Correspondingly, fracture energy per area is uniform (G_f) and can be obtained from the shape of the softening function as given in Equation (2) for ultimate strain in tension ε_{ult}. This also allows determining the shape parameter of the post-peak curve (b) from the fracture energy obtained in direct tensile testing based on the element size, a, Poisson's ratio, ν, tensile strain limit, ε_t, and the elasticity modulus E (Equation 3).

$$G_f = \frac{\sigma_t a\left(\exp\left(-2b\left(\varepsilon_{ult}-\varepsilon_t\right)\right) - 4\exp\left(-b\left(\varepsilon_{ult}-\varepsilon_t\right)\right) + 3\right)}{2b\left(1+\nu\right)} \tag{2}$$

$$b = 3/\left(\frac{2G_f\left(1+\upsilon\right)}{aE\varepsilon_t} - \varepsilon_t\right) \tag{3}$$

A number of validation problems were solved to demonstrate the applicability of the technique.[12] First, the uniaxial response of the model was compared to the well-known benchmark test of Gopalaratnam and Shah.[13] The tensile strength, modulus of elasticity, and the fracture energy of the specimen were reported as 3.41 MPa, 29.1 GPa, and 54 N/m, respectively, in this experiment. The satisfactory comparison of the load-displacement response to the experiment results using thee different meshes with 0.01, 0.007, and 0.005 m element sizes is presented in Figure 3A. Next, the 1:40 scaled concrete gravity dam experiment by Carpinteri et al.[14] is simulated. The specimen was loaded using a triangular load distribution in this test by displacement control until failure. Using the reported tensile strength, modulus of elasticity, and the fracture energy of 3.6 MPa, 35.7 GPa, and 184 N/m, respectively, the simulated load-CMOD response is compared to the experiment in Figure 3B. The results, obtained with element sizes of 0.05, 0.03, and 0.02 m, show good agreement with the experiment.

Finally, the mixed-mode failure of a double-edged notched specimen[15] is simulated using an element size of 0.005 m. The specimens given in this test series were applied tensile loading under pre-existing lateral load representing a complex failure state. The force–displacement response of two different specimens under 5 and 10 kN lateral loads was obtained and compared to test results in Figure 3C for tensile strength and fracture energy values of 2.55 MPa and 90 N/m, respectively. The results show satisfactory agreement with the testing.

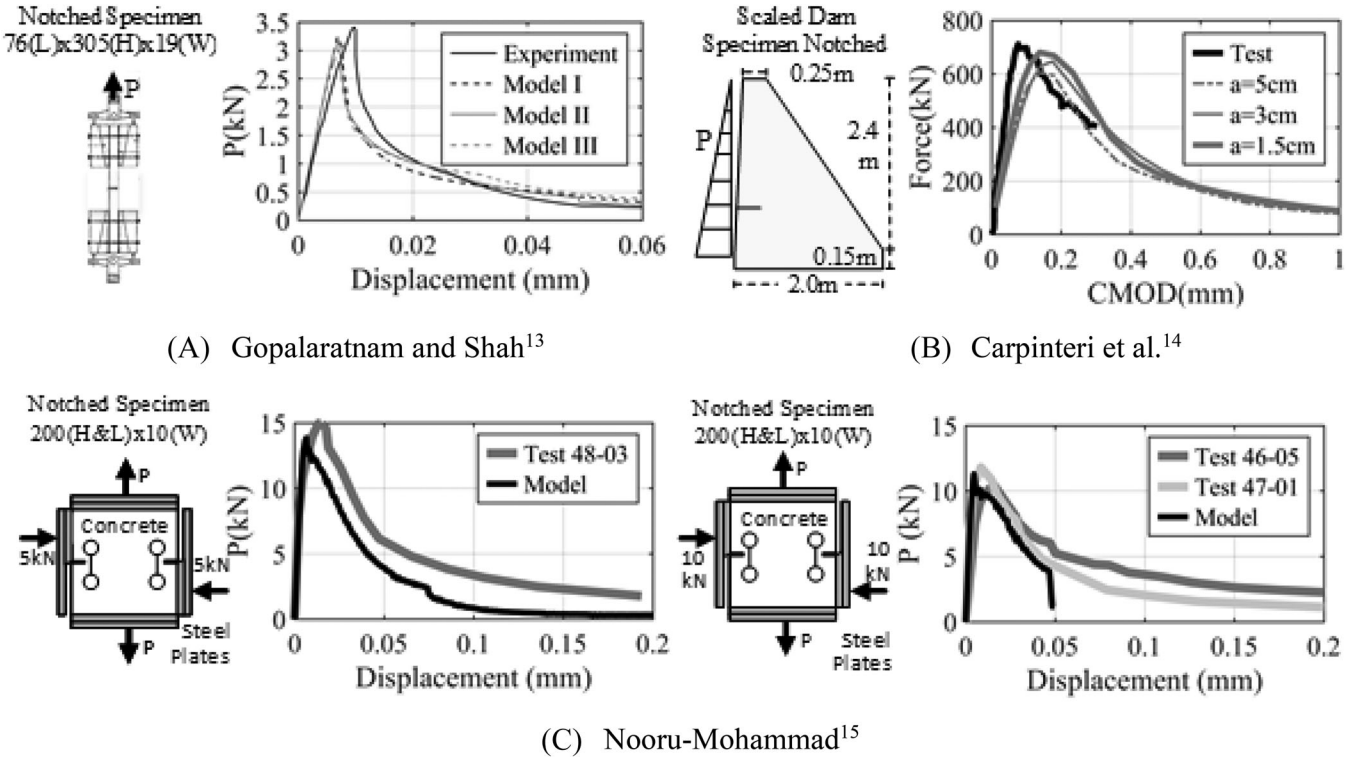

FIGURE 3 Model validation studies.

2.3 | Displacement/pressure based mixed finite element

A displacement/pressure based mixed finite element[16] has been coupled with the modified applied elements for modeling the reservoir behavior. The element, as shown in Figure 1B, has nine displacement degrees of freedom (marked with circles) and three pressure degrees of freedom (shown with triangles). The formulation yields a set of coupled equations below to be solved in terms of the solution vectors of displacement and pressure, $\hat{u}$ and $\hat{P}$, respectively, with M representing the mass term of the element and K_{uu}, K_{up}, K_{pu}, and K_{pp} represent the stiffness terms (Equation 4). For obtaining K_{uu} term of the stiffness matrix, the deviatoric part of the shape functions B (i.e., the derivatives of interpolation/shape functions) denoted as B_D is used.[17] For a finite bulk modulus, the pressure unknowns can be statically condensed out to simplify the solution of the equation (Equation 5).

$$\begin{bmatrix} M & 0 \\ 0 & 0 \end{bmatrix} \begin{bmatrix} \ddot{\hat{u}} \\ \ddot{\hat{P}} \end{bmatrix} + \begin{bmatrix} K_{uu} & K_{up} \\ K_{pu} & K_{pp} \end{bmatrix} \begin{bmatrix} \hat{u} \\ \hat{P} \end{bmatrix} = \begin{bmatrix} R \\ 0 \end{bmatrix} \tag{4}$$

$$M_{uu}\ddot{\hat{u}} + S_{uu}\,\hat{u} = R \tag{5}$$

where S_{uu} is calculated as $S_{uu} = -K_{up}K_{pp}^{-1}K_{pu}$. For an almost incompressible material (i.e., positive bulk, β, and shear modulus, G, with $\beta \gg G$), the displacement/pressure based mixed formulation fulfills the inf-sup condition eliminating the spurious zero-energy modes.[16]

For the validation of the implementation, the frequency response function of the idealized concrete gravity dam-reservoir system given in Fenves and Chopra[8] was regenerated (Figure 4A). The modulus elasticity, Poisson's ratio, and the dam concrete density were taken as 22.4 GPa, 0.2, and 2483 kg/m^3, respectively, while the acoustic wave speed, Poisson's ratio, and water density were assumed as 1477.2 m/s, 0.499, and 1000 kg/m^3, respectively. At the far end of the reservoir, the Sommerfeld radiation boundary condition was employed.[18] The damping coefficient, $q_s = 1/C_r$, is defined using the acoustic wave speed of water calculated as $C_r = \sqrt{\beta/\rho}$ with bulk modulus, β, and density, ρ of water.[19] The computed frequency response of the dam-reservoir system is compared to the benchmark solution obtained using the computer code EAGD84[20] in Figure 4B.

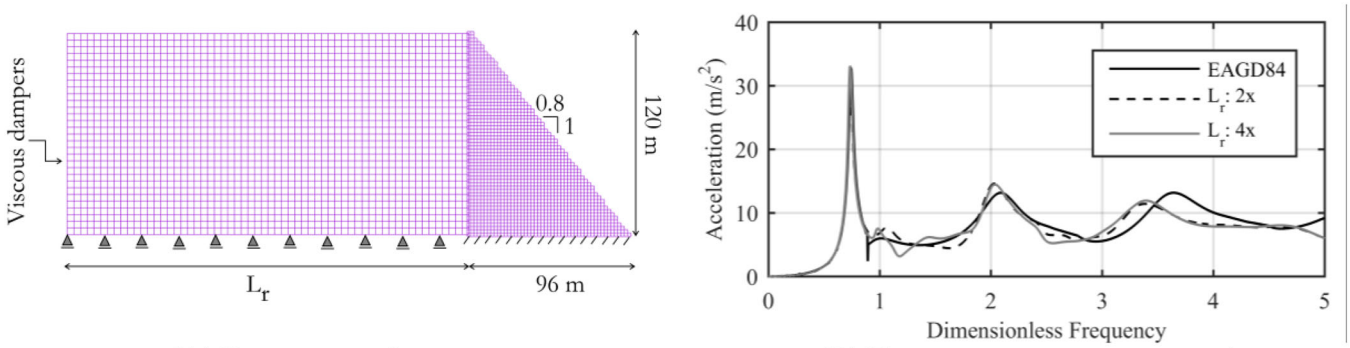

(A) Dam-reservoir system (B) Frequency response comparison

FIGURE 4 Frequency response of coupled Modified Applied Element Method (MAEM) – mixed reservoir element.

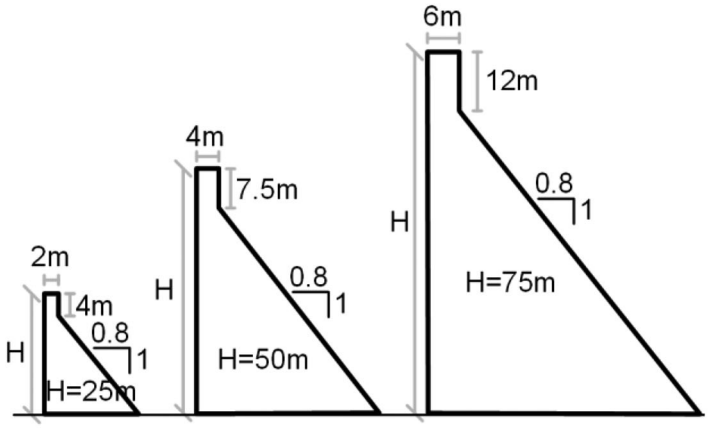

(A) Dam system geometries

	H=25 m	H=50m	H=75m
f_r(Hz)	15.6	7.5	4.9
f_1(Hz)	15.2	7.9	5.3
$\tilde{f}_1$(Hz)	12.3	6.3	4.1
$\tilde{f}_2$(Hz)	15.6	8.2	5.5
$\tilde{f}_4$(Hz)	31.2	20.8	15.1
$\tilde{\zeta}_1$(%)	4.7	4.6	4.6
$\tilde{\zeta}_2$(%)	5.9	6.5	6.3

(B) Modal frequencies and damping ratios

FIGURE 5 Generic dam systems.

3 | SYSTEM AND GROUND MOTION SELECTION

3.1 | Dam systems

The effect of vertical motions depends on the nature of the ground motions as well as the frequency response of the analyzed systems. Three different systems with heights of 25, 50, and 75 m are used to assess the relative differences of system response in the effects of vertical shaking (Figure 5A). These systems have generic cross-sections with a flat upstream (U/S) face and a downstream slope of 0.8(H)/1(V). The reservoir was assumed 2 m below the crest of the dam for all systems. The concrete monoliths were assumed to be built with roller-compacted concrete (RCC); the elasticity modulus, Poisson's ratio, tensile strength, and the fracture energy were assumed as 28 GPa, 0.2, 2.4 MPa, and 200 N/m, respectively. For the lift joints, in accordance with USACE,[21] the tensile strength and fracture energy were assumed as 1.4 MPa and 110 N/m, respectively. The reservoir was modeled with the mixed u/p elements given above; the acoustic wave speed, Poisson's ratio, and the density of water were taken as 1438.66 m/s, 0.4999, and 1000 kg/m^3, respectively.

The natural frequencies and the corresponding damping ratios were computed from the frequency response curves of the crest acceleration of the chosen systems. The frequencies corresponding to impounded reservoir (f_r), fundamental frequency of dam without the reservoir (f_1), and the first and second frequencies of the dam system with the reservoir ($\tilde{f}_1$ and $\tilde{f}_2$) are presented in Figure 5B. The damping ratios for the first two modes are also provided – these damping ratios were obtained using the full functional form of the half-power bandwidth method on the transfer functions for the crest acceleration response. For the bounding frequency values $f_{i,1}$ and $f_{i,2}$ corresponding to $1/\sqrt{2}$ times the mode resonant amplitude at either sides of the modal frequency peak f_i, Equation (6) was solved to determine the equivalent damping

FIGURE 6 Site location and major faults.

ratio for the *i*th mode.

$$\left(\frac{f_{i,2}}{f_i}\right)^2 - \left(\frac{f_{i,1}}{f_i}\right)^2 = 4\xi_i\sqrt{1-\xi_i^2} \tag{6}$$

The modal behavior of the dam-reservoir system is complex with coupling of the response in the horizontal and vertical directions. The fundamental frequency $\tilde{f}_1$ represents the dominant horizontal motion of the dam-reservoir system, the first bending mode, on which the effect of the horizontal excitation is more effective. The second frequency $\tilde{f}_2$ of the system corresponds to coupling of the system frequency with the impounded reservoir: this mode particularly reflects the effect of the vertical shaking on the dam horizontal motion due to hydrodynamic effects. Only the very high frequency $\tilde{f}_4$ represents the dominant vertical shaking corresponding to an elongation mode for the dam section, primarily affected by the vertical input.

3.2 | Seismic hazard

For the evaluation and design of dams, conducting nonlinear THA with a suite of ground motion records is the common approach. Regarding the selection of horizontal ground motion for nonlinear THA of dam structures, the conventional criteria given in the literature suggest the use of records that fairly represent the seismological and geological characteristics of the site, compatible with the hazard levels for a given set of return period events (e.g., USACE,[22] USBR[23]). The criteria for predicting the vertical motion and selecting compatible records for dam structures have been addressed little in the literature. Correspondingly, the typical practice was followed to select horizontal and vertical ground motion pairs. This requires site-specific assessment of the seismic demand along with the determination of appropriate vertical (V) to horizontal (H) demand ratios.

In order to determine the appropriate set of ground motions for analysis, first, a probabilistic seismic hazard analysis (PSHA) for a real dam site near eastern Istanbul was conducted. The location of the dam site (41.0758N, 29.1169E) is about 35 km away from the Princes Islands segment of North Anatolian Fault (NAF) in the Marmara Sea (Figure 6). The average shear-wave velocity measured at the top of 30 m soil (V_{S30}) is 760 m/s for the selected site, which is then used to generate the seismic scenarios for the site and ground motion selection. The use of (V_{S30}) is a practical necessity due to the lack of ground motions for sites classified with deeper investigations. Actually, for massive structures like concrete gravity dams, the stratum that should be considered for proper representation of response is much deeper than 30 m. The upper 30 m is usually softer than the underlying layers as shown with deep seismological surveys,[24] moduli and density increasing with depth.[25] However, even for sites classified by V_{S30}, motions for rigid foundation conditions pertaining to many dams (i.e., $V_{S30} > 2000$ m/s) are very rare leading to this practical choice and using reliable ground motion data in current databases classified with shear wave velocity in the first 30 m of the underlying layers.

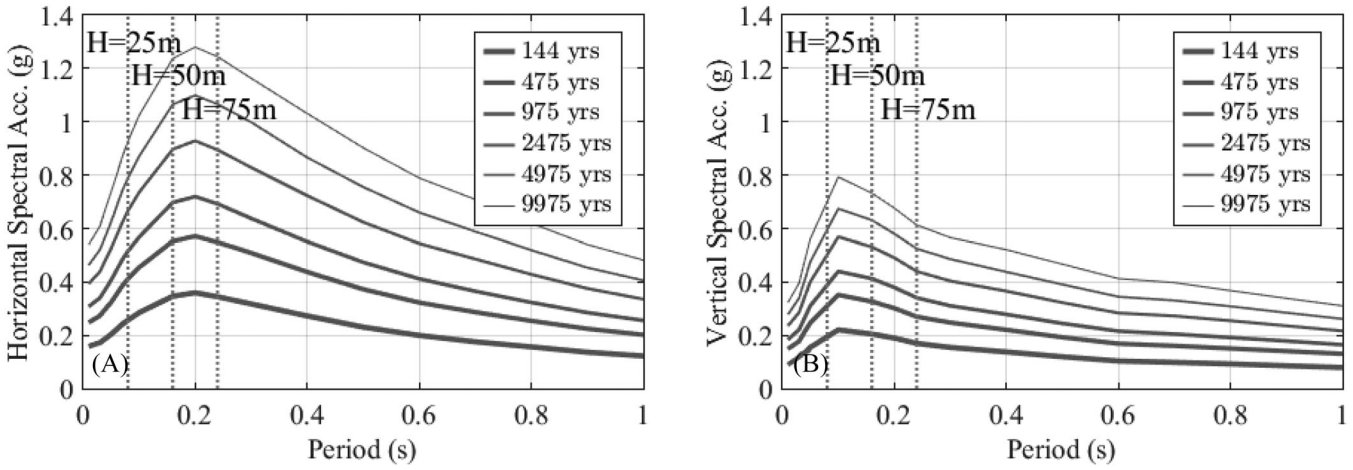

FIGURE 7 Probabilistic seismic hazard analysis (PSHA) based horizontal spectra and its vertical counterpart for six different return period values.

TABLE 1 Mean deaggregation results and the contribution of the major seismic source.

Return period (years)	Sa(0.16s)	$\overline{M}$	$\overline{R}$	$\overline{\varepsilon}$	Contribution of the Princes Islands segment (%)
144	0.351	7.08	38.5	0.87	65.7
475	0.553	7.11	35.5	1.44	75.4
975	0.697	7.13	34.3	1.75	79.4
2475	0.897	7.12	34.9	2.05	77.2
4975	1.065	7.16	32.9	2.33	84.9
9975	1.237	7.16	32.5	2.53	86.5

Figure 7 shows the PSHA-based UHS for 144, 475, 975, 2475, 4975, and 9975 years return periods. The expression for the vertical to horizontal component (V/H) ratio proposed by Akkar et al.[26] was used to establish the vertical spectrum ordinates at the different periods. The V/H ratio of Akkar et al.[26] relies on seismological parameters of the target scenario earthquake derived from the deaggregation of PSHA. The vertical spectrum consistent with the horizontal spectrum corresponding to the six different return periods considered in this study is shown in Figure 7. The fundamental frequencies of the dam systems are also marked separately in each spectrum. The deaggregation of the hazard at six return periods for the three dam systems yield moment magnitude values between 7.1 and 7.2 and source-to-site distance values ranging from 32 to 39 km. All the deaggregation results were fairly similar for different hazard levels and dam periods because the Princes Islands segment of NAF in the Marmara Sea is the major seismic source that primarily contributes to the hazard levels of engineering concern. The mean scenarios for the 50 m dam are listed in Table 1 for different levels of hazard. For example, the contribution of the strike-slip Princes Islands segment, strike-slip İzmit segment, and the normal faulting Çınarcık Basin of the NAF to the 475 years hazard is 75.4%, 14.0%, and 8.5%, respectively, whereas the contribution of other faults was found less than 1%.

3.3 | Ground motion selection

According to the deaggregation results, candidate records that have moment magnitude values between 6.5 and 7.7 and source-to-site distances (Joyner–Boore distance, R_{JB}) ranging from 0 to 100 km were selected from the PEER NGA-West2 (http://ngawest2.berkeley.edu) ground motion database. Despite the continuous growth of strong ground motions databases (PEER NGA-West2 Database includes more than 20,000 records from 600 different events), there are practical limitations and challenges in selecting a proper set of real records for such systems. The limited number of accelerograms of engineering significance satisfying all the constraints imposed by the site-specific hazard is still a major concern.

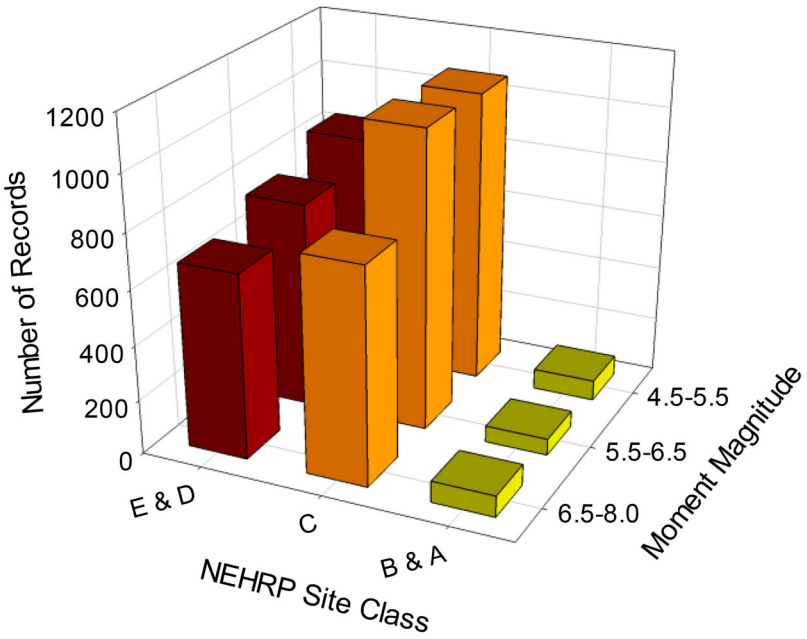

FIGURE 8 Number of available records in PEER NGA-West2 Database for different magnitude and site classes.

As mentioned before, this is particularly valid for dam structures located on rock sites. The number of available records (moment magnitude is larger than 4.5 and source-to-site distance is less than 100 km) in PEER Ground motion database, classified into three magnitude and site categories, are compared in Figure 8.

Records having V_{S30} values ranging from 600 to 1500 m/s were used to account for the site class information. As inferred from Figure 8, the V_{S30} criterion strictly limited the available number of candidate records. On the other hand, ground motion records having a lowest usable frequency larger than 1.5 Hz were excluded from the candidate library regarding the fundamental vibration frequencies of dam models. Records containing velocity pulses were also excluded from the candidate dataset. All these constraints yielded 364 accelerogram pairs (one horizontal and corresponding vertical component) from 21 events. Using each horizontal component of the records as an individual candidate is in line with former studies (e.g., Bernier et al.,[27] Soysal et al.[28]) on dam response. This approach doubles the number of candidate records increasing the possibility of having a better fit with the target hazard level.

Among 364 candidate ground motions, 40 pairs of unscaled accelerograms (40 horizontal and corresponding 40 vertical components) were selected considering the similarity between the horizontal and vertical mean spectra and the corresponding 475 years spectra. In selecting the records, the common approach is to use a period band ranging from $0.2T^*$ to $2.0T^*$, where T^* is the fundamental vibration period to consider higher mode effects and the period shift due to the inelastic response. Since the fundamental periods of three monoliths correspond to a relatively narrow period interval, a single spectral period band ranging from 0.01 to 0.6 s was used for all three dams. The statistical measure given in Jayaram et al.[29] was used to quantify the match between the mean spectrum of the set and the target spectrum. Equal weighting was used both for the horizontal and vertical fit with the corresponding target. In order to prevent the dominancy of records from one single event, Ay et al.[30] proposed one-third of the required number of records as the limiting value. Thus, the maximum number of records from the same event was limited to 13 in this study. The record name and horizontal component ($H1$ or $H2$), earthquake event, M_W, R_{JB} distance, V_{S30} information, and the main intensity parameters of 40 pairs of ground motion records selected are listed in Table 2. The moment magnitude of the final records ranges from 6.6 to 7.6, whereas the source-to-site distance values are between 0 and 33.3 km. The minimum and maximum V_{S30} values of the selected records are 616 and 996 m/s, respectively. The horizontal and vertical acceleration spectra of these 40 records are presented in Figure 9 along with the mean and the target response spectrum. The unscaled 40 record pairs (Table 2) compatible with horizontal and vertical 475 years return period target spectrum were scaled in amplitude to match with other ground motion levels. Amplitude scaling of motions to meet the target spectra was conducted carefully with factors of 0.64, 1.26, 1.63, 1.95, and 2.29 for the 144, 975, 2475, 4975, and 9975 years return period ground motion level, respectively. The same suite of records modified with different scaling factors corresponding to different hazard levels is fairly acceptable for the given dam site since the hazard is mainly governed by the same seismic source as shown in Table 1.

TABLE 2 Selected ground motion set, record, event name and corresponding parameters

Record	Earthquake	M_W	R_{JB} (km)	V_{S30} (m/s)	$PGA_{Hor.}$ (g)	$PGA_{Ver.}$ (g)	Arias int. (m/s)	CAV (m/s)	T_p (s)
763_H2	Loma Prieta	6.9	9.2	730	0.33	0.19	0.70	5.14	0.18
769_H2	Loma Prieta	6.9	17.9	663	0.17	0.10	0.45	5.58	0.24
801_H1	Loma Prieta	6.9	14.2	672	0.28	0.23	1.31	9.78	0.18
801_H2	Loma Prieta	6.9	14.2	672	0.26	0.23	1.00	8.73	0.12
809_H1	Loma Prieta	6.9	12.2	714	0.31	0.22	0.85	6.78	0.18
989_H1	Northridge-01	6.7	9.9	740	0.22	0.15	0.62	6.10	0.42
1091_H1	Northridge-01	6.7	23.1	996	0.15	0.09	0.37	4.55	0.38
1091_H2	Northridge-01	6.7	23.1	996	0.14	0.09	0.32	4.26	0.20
1161_H1	Kocaeli-Turkey	7.5	7.6	792	0.26	0.19	0.55	5.24	0.34
1161_H2	Kocaeli-Turkey	7.5	7.6	792	0.14	0.19	0.32	4.47	0.44
1165_H1	Kocaeli-Turkey	7.5	3.6	811	0.17	0.14	0.56	6.81	0.28
1165_H2	Kocaeli-Turkey	7.5	3.6	811	0.23	0.14	0.81	7.79	0.28
1350_H1	Chi-Chi-Taiwan	7.6	33.3	665	0.20	0.10	0.60	8.12	0.14
1350_H2	Chi-Chi-Taiwan	7.6	33.3	665	0.17	0.10	0.72	9.16	0.14
1521_H2	Chi-Chi-Taiwan	7.6	0.0	672	0.23	0.19	1.55	14.62	0.24
1551_H2	Chi-Chi-Taiwan	7.6	9.8	653	0.21	0.11	1.60	18.54	0.42
1618_H1	Duzce-Turkey	7.1	8.0	638	0.16	0.06	0.45	6.14	0.26
1787_H1	Hector Mine	7.1	10.4	726	0.27	0.15	0.83	7.96	0.22
3943_H1	Tottori-Japan	6.6	9.1	617	0.15	0.16	0.35	5.94	0.26
3943_H2	Tottori-Japan	6.6	9.1	617	0.27	0.16	0.38	5.96	0.20
3954_H2	Tottori-Japan	6.6	15.6	967	0.23	0.14	0.48	5.80	0.20
4213_H2	Niigata-Japan	6.6	25.3	655	0.28	0.09	0.46	6.08	0.18
4841_H2	Chuetsu-oki-Japan	6.8	20.7	655	0.22	0.05	0.74	7.56	0.26
4842_H1	Chuetsu-oki-Japan	6.8	18.6	655	0.26	0.13	0.59	6.43	0.22
4843_H1	Chuetsu-oki-Japan	6.8	18.2	640	0.19	0.07	0.71	8.46	0.64
4843_H2	Chuetsu-oki-Japan	6.8	18.2	640	0.19	0.07	0.51	7.44	0.50
4858_H1	Chuetsu-oki-Japan	6.8	25.4	640	0.21	0.07	0.54	6.62	0.34
4858_H2	Chuetsu-oki-Japan	6.8	25.4	640	0.25	0.07	0.49	6.59	0.36
4864_H1	Chuetsu-oki-Japan	6.8	4.7	655	0.28	0.17	1.88	13.16	0.32
4869_H2	Chuetsu-oki-Japan	6.8	23.6	640	0.21	0.07	0.50	7.81	0.20
5474_H2	Iwate-Japan	6.9	26.0	640	0.18	0.14	0.80	10.19	0.08
5618_H1	Iwate-Japan	6.9	16.3	826	0.23	0.20	1.31	14.32	0.36
5618_H2	Iwate-Japan	6.9	16.3	826	0.29	0.20	1.36	14.74	0.14
5806_H1	Iwate-Japan	6.9	22.4	655	0.24	0.12	0.73	8.58	0.20
5806_H2	Iwate-Japan	6.9	22.4	655	0.19	0.12	0.62	8.13	0.34
5809_H1	Iwate-Japan	6.9	17.3	655	0.24	0.14	0.94	9.00	0.14
5809_H2	Iwate-Japan	6.9	17.3	655	0.22	0.14	0.85	8.29	0.30
5815_H1	Iwate-Japan	6.9	22.4	655	0.19	0.17	0.93	9.82	0.30
6928_H1	Darfield-New Zealand	7.0	25.2	650	0.24	0.16	0.68	7.40	0.16
6928_H2	Darfield-New Zealand	7.0	25.2	650	0.36	0.16	0.69	7.10	0.20

Concrete dams are designed for different seismic levels corresponding to the associated hazard and consequences of damage on the system. These are typically provided as OBE, MDE, and MCE in the guidelines.[23] For the 25 m dam monolith, these levels were assumed to correspond to 2475, 4975, and 9975 years events, respectively. These correspond to return periods usually assumed for European dams. For the 50 m dam monolith, 475, 2475, and 4975 years events were used. For the 75 m dam, 144, 475, and 2475 years events typically chosen in seismically very active countries like Turkey were used.

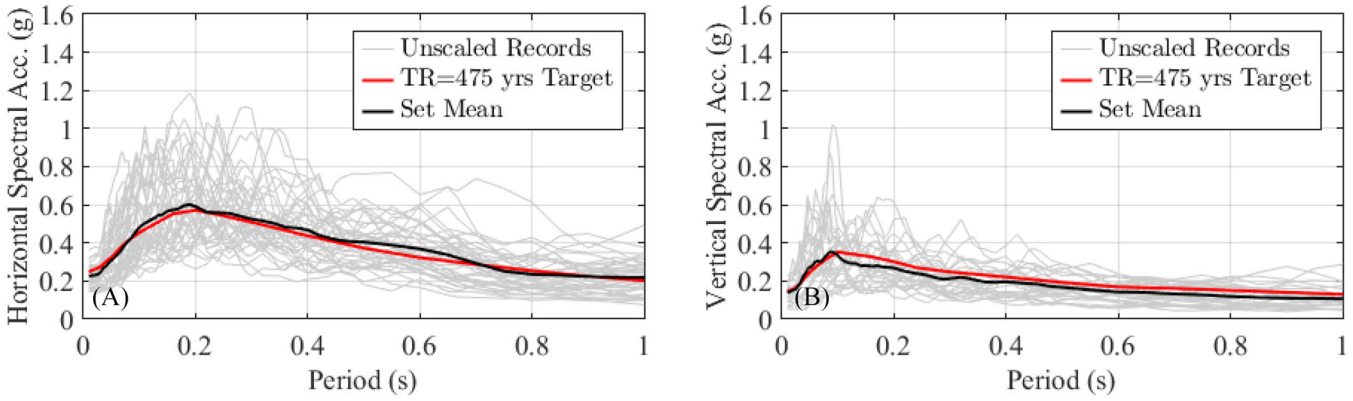

FIGURE 9 Acceleration spectra of the selected records, their mean, and corresponding target spectrum for 475 years return period.

The utility of the use of different levels of motion is two-folds; first, the systems are tested at different levels of demand enabling seeing the coupling of nonlinearity and the effects of vertical motion. Secondly, it allows including the level of shaking in comparisons of H and $H + V$ analyses. The response quantities can also be compared in the linear range as well: as given below, the 25 m dam monolith did not suffer damage for the selected motion levels.

4 | THE EVALUATION OF THE EFFECT OF VERTICAL SHAKING ON EDPS

4.1 | Engineering demand parameters

Two types of seismic demand measures were used to assess the effect of vertical motions on the dam behavior. The first group corresponding to classical demand measures was the displacement and acceleration response at the crest of the dam. The maximum horizontal and vertical displacement/acceleration values were obtained for each system and ground motion with and without the vertical excitation component. The second group of demand measures used were the damage related quantities. The maximum crack width at the base, the maximum total crack width on the U/S face, the maximum length of crack at the base of the system as well as the post-seismic factor of safety values at the base and the neck of the system were obtained from the simulations. Factor of safety against sliding in post-seismic state (FSS) was computed using Equation (7) in

$$\mathrm{FSS} = \frac{(\tan(\varphi) * (N - U) + c * A_{\mathrm{int}})}{F_{\mathrm{lat}}} \tag{7}$$

which N, U, F_{lat}, and A_{int} represent the normal, uplift, horizontal force, and the intact area at the sliding plane, respectively. Resistance is determined by the coefficient of friction and cohesion at the interface, expressed as $\tan(\varphi)$ and c, respectively. The angle of friction (peak) at the sliding planes was assumed conservatively as 45° while cohesion value was assumed as 2.0 MPa.

4.2 | Analysis results

Dam-reservoir system produces a complex interaction investigated for different levels of excitation (seismic level) and ground motions. Vertical motion affects the system through vertical shaking of the system as well as through the vibration modes of the impounded reservoir. The hydrodynamic forces in the horizontal direction due to the vertical motion was deemed significant in very early work.[31] In order to evaluate this effect, the hydrodynamic forces on the dam due to the horizontal ($\tilde{F}_0^x$) and vertical components ($\tilde{F}_0^y$) were computed using Equation (8) and compared. In this equation,[1] $\tilde{p}_0^l$ represents the hydrodynamic pressure on the upstream of the monolith due to motion in l direction at the angular frequency ω. These forces due to rigid body movement of the monolith are frequency dependent; consequently, the frequency dependent hydrodynamic total force was multiplied by the frequency response of the chosen ground motions and

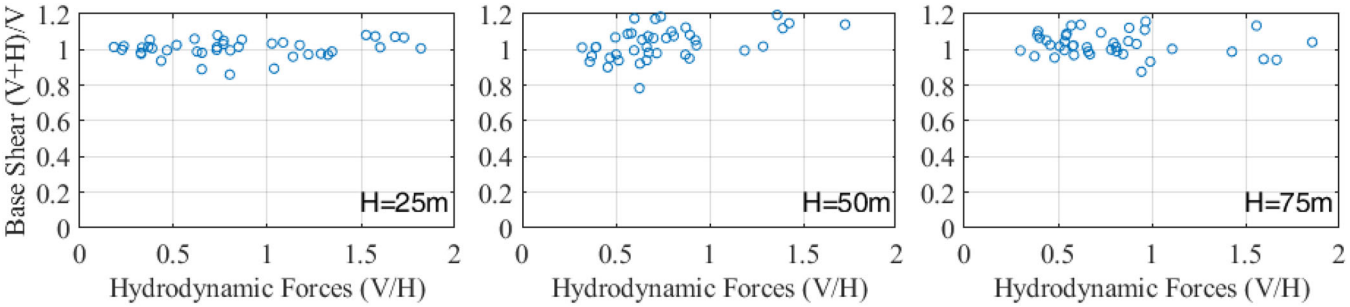

FIGURE 10 Base shear for analysis with and without vertical component (V), relationship with hydrodynamic forces due to vertical and horizontal component of ground motion.

TABLE 3 Statistics for engineering demand parameter (EDP) with and without vertical ground motions, 75 m monolith

	TR144		TR475		TR2475	
	H	$H+V$	H	$H+V$	H	$H+V$
Hor. acc. (m/s^2)	9.93 (0.29)	11.21 (0.29)	15.18 (0.29)	17.158 (0.27)	22.63 (0.24)	24.31 (0.22)
Hor. disp. (m)	1.8 (0.25)	1.9 (0.25)	2.7 (0.28)	2.9 (0.28)	4.5 (0.29)	4.7 (0.28)
Ver. acc. (m/s^2)	3.37 (0.42)	4.39 (0.39)	6.28 (0.34)	7.68 (0.31)	10.09 (0.26)	12.10 (0.27)
Ver. disp. (cm)	0.4 (0.34)	0.4 (0.36)	0.7 (0.44)	0.8 (0.43)	1.6 (0.42)	1.7 (0.38)
Base crack width (mm)	0.97 (0.25)	0.99 (0.25)	1.39 (0.23)	1.44 (0.24)	1.74 (0.19)	1.66 (0.22)
Base crack length (m)	12.07 (0.29)	12.09 (0.28)	17.47 (0.21)	17.66 (0.21)	25.01 (0.20)	25.63 (0.20)
U/S crack width (mm)	1.86 (0.82)	2.36 (0.81)	6.39 (0.66)	7.75 (0.56)	17.71 (0.5)	19.73 (0.43)
Post-seismic FSS_{Base}	4.23 (0.08)	4.23 (0.08)	3.80 (0.11)	3.85 (0.12)	3.19 (0.19)	3.17 (0.18)
Post-seismic FSS_{Neck}	6.99 (1.15)	4.74 (1.06)	2.88 (0.62)	2.60 (0.36)	2.51 (0.15)	2.54 (0.16)

the time domain maximum quantities were obtained by the inverse Fourier transform.

$$\tilde{F}_0^l = \int_0^H \tilde{p}_0^l(0,\omega,y)\,dy \tag{8}$$

Base shear is a traditionally important demand parameter; the relationship of hydrodynamic forces and base shear is evaluated first to discern the effect of vertical motions on the response. Base shear obtained with and without the vertical component of motion and the corresponding ratio of the hydrodynamic forces computed from Equation (8) is presented in Figure 10 for each ground motion for the three systems considered. In the average, the hydrodynamic force due to vertical component was at 75% of the horizontal counterpart although there are motion sets with significantly higher (1.8×) and lower (0.3×) ratios. The relative effect on the seismic base shear, on the other hand, is not strong: higher vertical motion contribution to hydrodynamic force does not directly correspond to higher base shear. This finding supports the conclusion presented in Ref. [32] regarding the phase response greatly moderating the contribution of vertical ground motion to the total response.

The aforementioned EDPs pertaining to performance were obtained for the selected systems from these analyses, with and without the vertical component of motion, at different seismic levels. The statistics for the results are displayed in Table 3 computed assuming log-normal distribution for the outcome. The geometric mean and log-standard deviations (in parenthesis) are shown separately. Selected EDPs are also shown for the 75 m tall system in Figure 11 for the for the 144-, 475-, and 2475-years earthquake events.

The mean response for the $H + V$ case was generally larger as shown in Table 3 and Figure 11. The mean demand increased consistently for crest acceleration demands as well as the base crack width and length. The increase for the displacement response and total U/S crack width was much more with the seismic level. The factor of safety values at the base reduce for increasing seismic level with little effect of vertical motion. Factor of safety at the neck is markedly affected by vertical motion for the smallest event but this effect diminishes for increasing seismic level. For the 2475 year event, the mean factor of safety values, with and without vertical shaking, were similar.

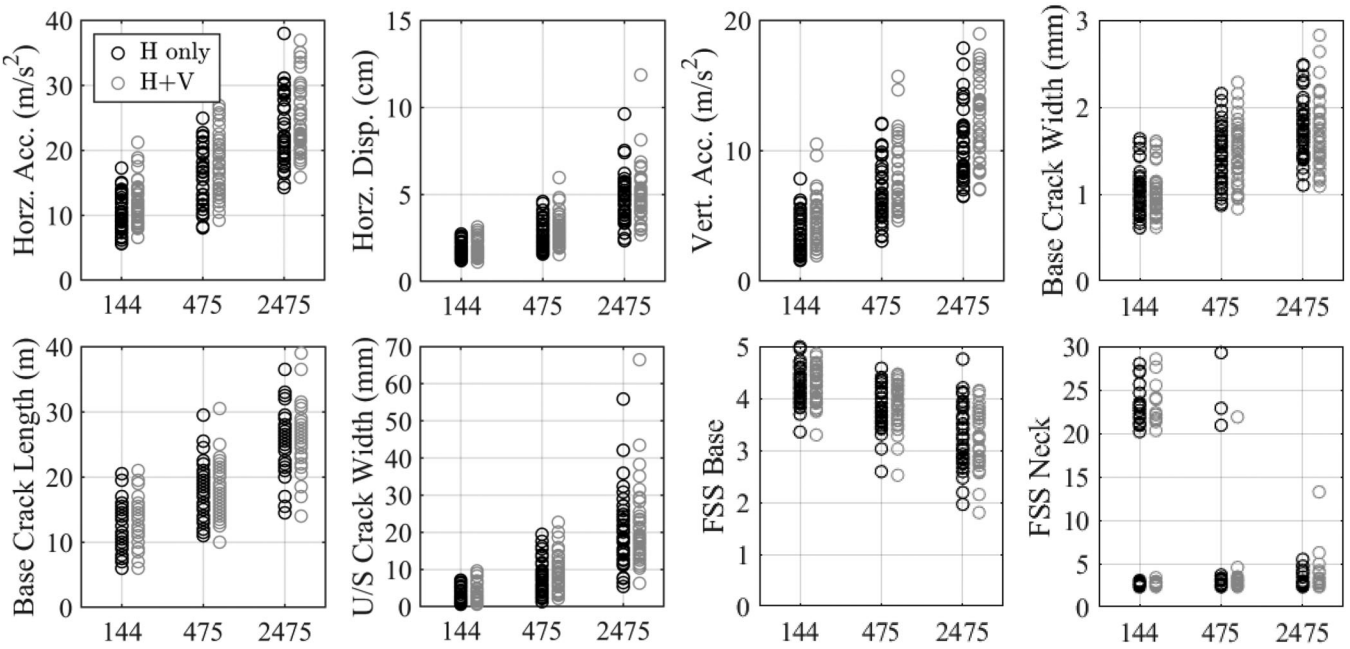

FIGURE 11 Demand measures for the 75 m dam monolith.

Regarding the dispersion in the EDP estimates, mixed results corresponding to damage accumulation was obtained. The dispersion values reduced with increasing shaking level for the acceleration, crack width EDPs, and post-seismic FSS at neck, showing the effect of the accumulated damage on the system. The dispersion in the horizontal displacement and post-seismic base FSS increased with shaking. The trend in dispersion was uneven for the vertical displacement of the crest. For analysis with $H + V$ components, the dispersion was obtained mostly similar to H only analyses.

4.3 | Effect of vertical motions

The effects of the vertical motions were next investigated by comparing the results of H and $H + V$ analyses with the "skew" curves. The one-to-one comparison between the demand values obtained from H and $H + V$ analyses are presented in Figure 12 for the 75 m dam at the 2475 year earthquake event. The red line in the figures shows theoretical identical response for analyses with and without vertical ground motions: that is, the results for the $(H + V)$ case should rest on this line if the vertical motion is not effective. The black line shown on these plots is the fit obtained through linear regression on H and $H + V$ cases showing the correspondence between the cases in an average sense. For example, the horizontal acceleration was obtained 6% larger in $(H + V)$ cases compared to analyses using horizontal motion only. The trend was similar for the conventional demand measures with the maximum difference in the vertical acceleration demand.

For the damage-based demand measures, the results were mixed. Considering the vertical component of the motion led to lower maximum crack width prediction for the base crack in an average sense. There is a significant dispersion in this data showing the vertical motion is very effective on this demand parameter and the response depends on the phasing of both components. The length of the base crack does not appear to depend on the vertical motion in this case, with high correspondence between the H and $H + V$ cases and small dispersion of the results. The total damage on the upstream face of the monolith, on the other hand, increases with consideration of the vertical motion. The dispersion also is biased toward $H + V$ side: vertical motion is likely to lead to more damage compared to reducing it. The effect of vertical motion on the FSS was small for the base and neck sections, however, the behavior was different. At this level of shaking (TR2475), a through crack formed at the neck of the dam for H only shaking, the vertical motions' effect on increasing damage was consequently limited.

The demand measures were obtained for all three systems considered in a similar fashion to the results displayed in Figure 12. These results are summarized in a tabular form in Table 4. The factors (a) given in the table represent the ratio of the demand between $(H + \mathrm{V})$ and horizontal only (H) analyses. The corresponding R^2 value shows the associated confidence in this estimate and the dispersion in the results.

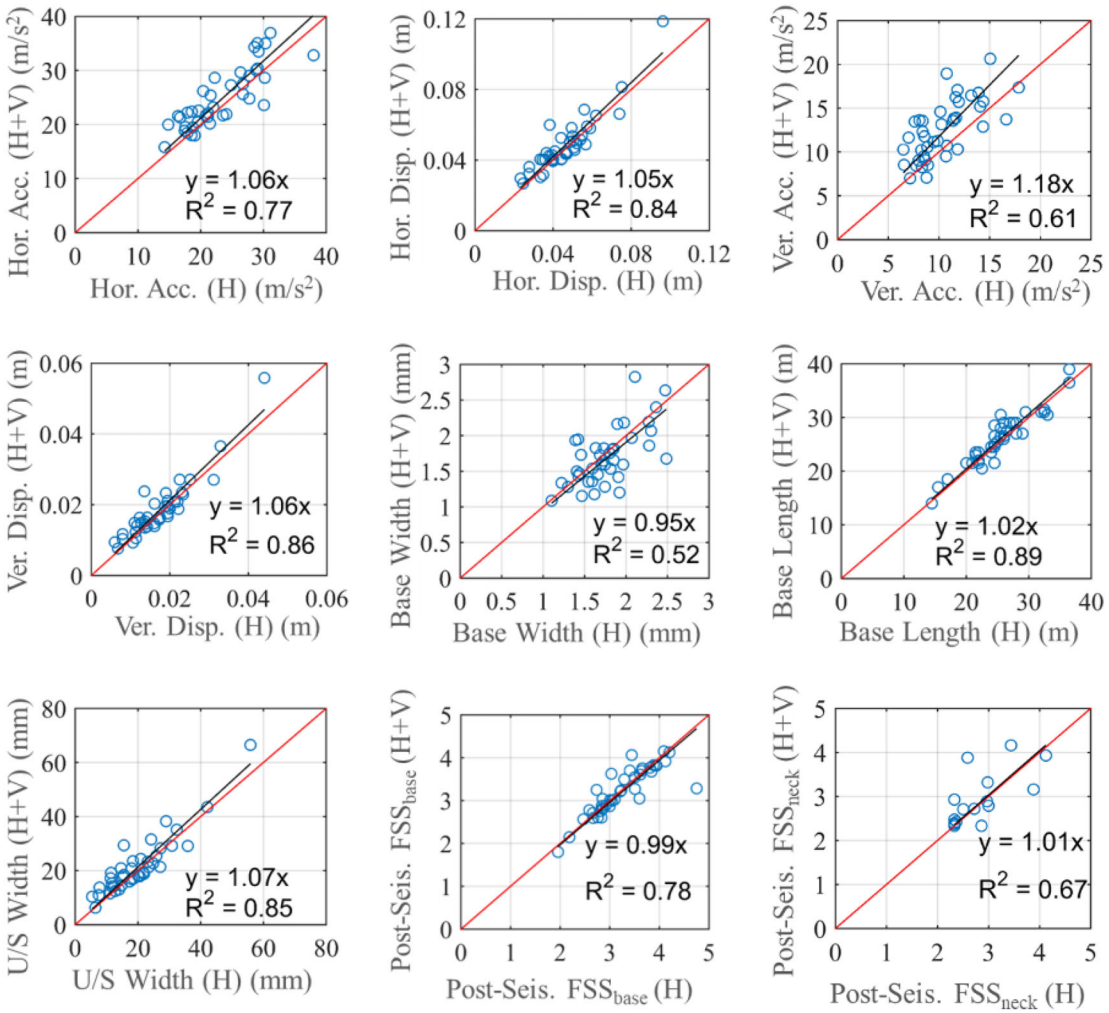

FIGURE 12 Seismic demand measures, with/without vertical effect for the 75 m dam monolith for TR2475.

TABLE 4 The effect of vertical motion on engineering demand parameters (EDPs) expressed in factor a (w vert. = w/o vert.x a) and confidence in the estimate (R^2).

Dam height	***H* = 25 m**						***H* = 50 m**						***H* = 75 m**					
Return period	**2475**		**4975**		**9975**		**475**		**2475**		**4975**		**144**		**475**		**2475**	
EDP	***a***	***R*²**	***a***	***R*²**	***a***	***R*²**	***a***	***R*²**	***a***	***R*²**	***a***	***R*²**	***a***	***R*²**	***a***	***R*²**	***a***	***R*²**
Hor. crest acc.	1.16	0.87	1.17	0.85	1.13	0.81	1.09	0.87	1.10	0.82	1.11	0.84	1.12	0.78	1.11	0.79	1.06	0.77
Hor. crest dis.	1.06	0.91	1.08	0.91	1.07	0.86	1.04	0.94	1.06	0.97	1.04	0.96	1.05	0.81	1.07	0.80	1.05	0.84
Ver. crest acc.	1.18	0.81	1.14	0.86	1.11	0.80	1.20	0.83	1.16	0.79	1.19	0.81	1.22	0.63	1.17	0.65	1.18	0.61
Ver. crest dis.	1.08	0.94	1.06	0.88	1.07	0.82	1.05	0.92	1.07	0.97	1.05	0.95	1.11	0.74	1.12	0.79	1.06	0.86
Base crack width	–	–	–	–	–	–	1.04	0.71	1.03	0.59	1.03	0.53	1.01	0.78	1.02	0.58	0.95	0.52
Base crack length	–	–	–	–	–	–	1.03	0.92	1.01	0.95	1.03	0.94	1.00	0.93	1.01	0.90	1.02	0.89
U/*S* crack width	–	–	–	–	–	–	1.03	0.89	1.09	0.96	1.07	0.94	1.15	0.79	1.09	0.83	1.07	0.85
Post-seismic FSS_{Base}	–	–	–	–	–	–	1.00	0.70	0.98	0.55	1.00	0.69	1.00	0.87	1.01	0.80	0.99	0.78
Post-seismic FSS_{Neck}	–	–	–	–	–	–	0.80	0.68	0.99	0.78	1.01	0.76	0.68	0.51	0.42	0.47	1.01	0.67

The results for the 25 m monolith were different compared to the other cases as the relative squat system in this geometry and the corresponding low frequency led to a low demand/capacity ratio. At the demand levels considered, the system did not suffer significant damage. Horizontal and vertical accelerations at the crest were obtained roughly 15% more for cases including vertical shaking. The displacements, on the other hand, were obtained 6%−8% more. The R^2 values were relatively high for these estimates, slightly reducing for the 9975 years event likely showing the onset of damage on this system.

For the 50 m monolith, the system suffered minor damage at the lowest level of shaking considered, coinciding with the OBE designation in the design codes. A more complex modal response was evident in this case. For the $H + V$ cases, horizontal crest acceleration was obtained 9% greater compared to a 20% difference in the vertical acceleration. The crest displacement demands were obtained 5% more for the $H + V$ cases compared to the H only cases. For the 2475 and 4975 years events, the factors among $H + V$ and H only cases for the acceleration and displacement demand values were obtained similarly. In contrast to mostly linear response at 475 years design level, some of the ground motions were damaging in the 2475 years case, while many led to damage in the 4975 years one. Corresponding damage accumulation, on the other hand, shows similar response. The base crack length and width changed 3% including the vertical component of the motion in the analysis. The effect on total damage was more significant. On average, 9% more damage was observed including vertical motions in the analysis for the 2475 years scenario. For the 4975 years case, the increase was somewhat smaller, at 7%. This corresponds to the increased likelihood of already strong horizontal shaking damaging the system at this level: vertical motions' effect was reduced. This trend is also evident in the factor of safety values at the neck of the dam. Including vertical motion led to smaller FSS for lower level of shaking while the effect was reduced for the 2475 and 4975 year cases.

The complete results for the 75 m monolith, presented in Figures 11, 12 for the 2475 year event, are summarized in Table 4. The increase in the horizontal and vertical crest accelerations considering the vertical component of shaking was similar to the previous case, around 10% and 20%, respectively. The horizontal and vertical crest displacements increased by around 5% and 10% in this case. Notably, the factors for the 2475 year event were somewhat lower, showing the vertical motions' effect reducing for this level causing consistently high damage on the system. The factors for the base crack width at different levels of motion demonstrate this response: considering vertical motion led to a 5% lower prediction for this quantity in an average sense with a marked increase in the dispersion. The base crack length was not affected from the consideration of the vertical shaking. Finally, the effect of the vertical motions on the total damage quantified as U/S crack width on the system decreased as the shaking levels increased. For the lowest level event, the increase in the damage was predicted at around 15% considering the vertical motion. Only a 7% increase was observed at the highest level of shaking. The effect on the extent of cracking on the neck was evident: marked reduction in ratios for FSS_{neck} for the 144 and 475 year events showed the vertical motion significantly affecting the cracking at the neck. The vertical motion did not include overall trend for FSS_{base} while increasing the dispersion in the results.

4.4 | Ground motion selection and vertical motions' effects

4.4.1 | Alternative target spectrum definitions

The effect of target spectrum definition on the coupled horizontal + vertical motion response was evaluated using two alternative target spectra and selecting motions accordingly. These are the conditional spectrum based on average spectral acceleration[33] and the UHS based on a PSHA conducted with vertical ground motion prediction equations. The conditional spectrum based on average spectral acceleration (CS(AvgSA)) for horizontal motion is calculated as compatible with the PSHA results, given in Section 3.2. For the logarithmic mean of the vertical conditional spectrum, the V/H prediction proposed by Akkar et al.[26] was used as given in Equation (9). This equation corresponds to a simplified approach that ignores the correlation of the ground motion variability between the horizontal and vertical motion (Gülerce and Abrahamson,[34] Akkar et al.[26]) but can fairly represent the mean of a vertical target for the evaluation of CS(AvgSA) on the effect of vertical motion on dam response. The variance of the vertical spectrum was calculated by Equation (10). Further details of calculation for mean and variance of horizontal ($CS(AvgSA)_H$) and vertical ($CS(AvgSA)_V$) target spectrum can be found in Kohrangi et al.,[33] Gülerce and Abrahamson,[34] and Akkar et al.[26]

$$\mu_{\ln CS(AvgSA)_V} = \mu_{\ln CS(AvgSA)_H} + \mu_{\ln(V/H)} \tag{9}$$

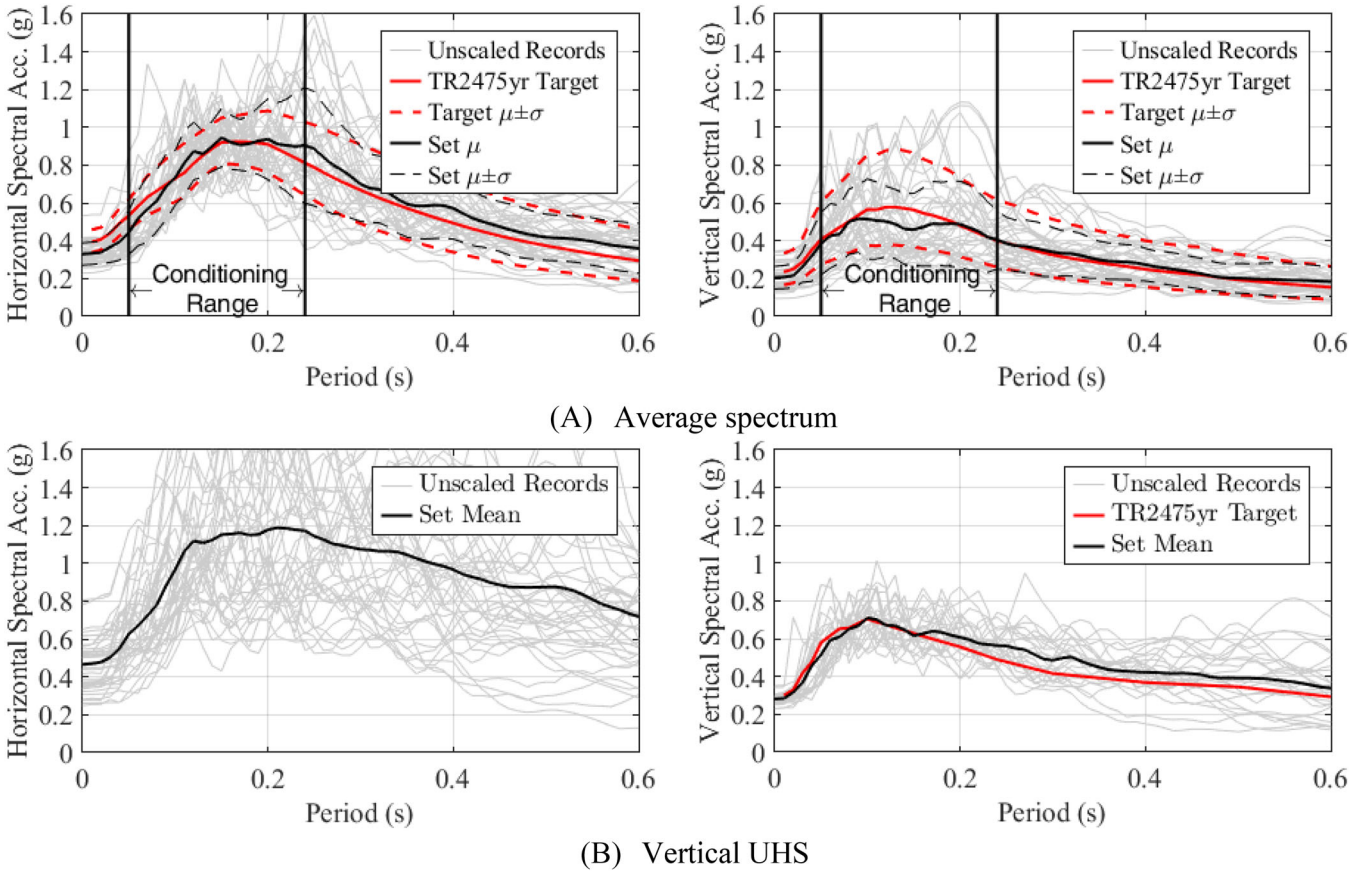

FIGURE 13 Alternative target spectrum definitions (average spectrum and vertical UHS) and selected sets.

$$\sigma^2_{\ln CS(AvgSA)_V} = \sigma^2_{\ln CS(AvgSA)_H} + \sigma^2_{V/H} + 2\rho_{H,V/H} \cdot \sigma_{\ln CS(AvgSA)_H} \cdot \sigma_{V/H} \tag{10}$$

Figure 13A shows the target horizontal and vertical CS(AvgSA), the spectra of the suite of records, their mean, and the ±standard deviation for horizontal and vertical motion. For dam response, the first four modes were taken into account (Figure 5B). Considering also the period elongation due to the inelastic behavior, conditioning period range was taken from T_4 to $1.5T_1$ (i.e., 0.05–0.24 s). Next, 40 pairs of records whose horizontal and vertical components match with $CS(AvgSA)_H$ and $CS(AvgSA)_V$, respectively, were selected.

The UHS for vertical acceleration response was computed from vertical GMPE-based PSHA (Figure 13B). The deaggregation results of vertical PSHA gave similar moment and distance values. Similar to the procedure described in Section 3.3, ground motion records are selected from a candidate set compatible with the deaggregation results, but only the vertical UHS is considered as the target. The spectra of the horizontal components of these motions and their mean (black solid line) are also presented in the same figure.

The results for the average design spectrum and the UHS is compared in Table 5 for the 50 m dam monolith and the 2475 year return period event. For the selected EDPs, the ratio of results with coupled $H + V$ analysis to H only case are provided as before. For most of the EDPs, the response was similar. Minor reductions of the $H + V$ response with respect to H only was observed for the base crack related quantities. The most prominent effect of the use of average spectrum on the $(H + V)/(H)$ quantity appears to be on the dispersion in the indicated relationship. The variability introduced by the ground motion significantly decreased the R^2 values for all EDPs except for the base crack EDPs. On the overall, the use of average spectrum minorly reduced the effect of the vertical motions on the considered EDPs in a mean sense, while increasing the variability in the response.

The factors and related R^2 values, obtained with the use of vertical target spectrum as the main seismic hazard output, were also compared to former results in Table 5. In this case, the effect of vertical motion on the results was very similar to the use of horizontal UHS as a target, except for the vertical crest acceleration EDP. The R^2 values were also obtained very similar to the horizontal UHS case.

TABLE 5 Comparison of the effect of coupled horizontal + vertical motions, UHS versus average design spectrum for motion selection

	Horizontal UHS		Average spectrum		Vertical UHS	
Seismic demand	**Factor (a)**	**Conf. (R^2)**	**Factor (a)**	**Conf. (R^2)**	**Factor (a)**	**Conf. (R^2)**
Hor. crest acc.	1.1	0.82	1.06	0.39	1.1	0.84
Hor. crest disp.	1.06	0.97	1.05	0.61	1.07	0.96
Ver. crest acc.	1.16	0.79	1.12	0.39	1.11	0.72
Ver. crest disp.	1.07	0.97	1.08	0.54	1.08	0.95
Base crack width	1.03	0.59	0.96	0.44	1.04	0.76
Base crack length	1.01	0.95	0.99	0.84	1.00	0.96
U/S crack width	1.09	0.96	1.08	0.52	1.1	0.94
Post-seismic FSS_{Base}	0.98	0.55	0.98	0.57	1.00	0.61
Post-seismic FSS_{Neck}	0.99	0.78	0.88	0.59	0.96	0.87

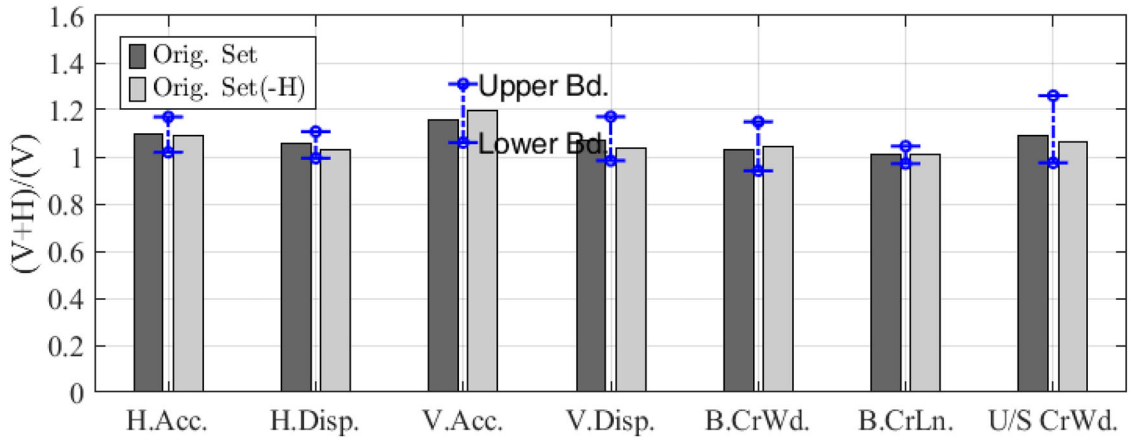

FIGURE 14 Direction effect on the effects of vertical motion on selected engineering demand parameters (EDPs).

4.5 | Direction effect on $V + H$ effects

The direction of loading is important for concrete gravity dams as the systems are designed for the critical effects of hydrostatic loading on the upstream side.[28] In order to see the effect of direction of the ground motions coupled with vertical motion component, the EDPs were obtained for the original suite, with altered horizontal motion direction, for the 50 m monolith at the 2475 return period. The direction of the vertical motions was not changed considering the polarity relationship between the horizontal and vertical components of the motion. From the original set (set 1) and the modified original set comprised with direction change of horizontal motions (set 2), two other sets were formed. The first one was comprised of motions providing the larger $(V + H)/V$ ratio from set 1 and 2 for each motion, while the second one was formed with motions yielding the lower. The results obtained from these four sets are compared in Figure 14. The original set and the set with negative horizontal component generally yielded similar factor and R^2 values. The other sets form the upper and lower bound around these two sets: the largest effect of vertical motion was on the vertical acceleration as before (factor at 1.3). Upstream crack width was also affected, maximum and minimum factors obtained at 1.26 and 0.97, respectively. The effect of direction coupled with vertical motion was small for horizontal acceleration, displacement and predicted base crack length.

5 | CONCLUSIONS

In this study, the significance of the vertical motion component in the seismic analysis of concrete gravity dams was investigated considering conventional and damage related demand quantities to assess dam behavior. The effect was quantified

for different gravity dam systems in order to consider the variability of modal properties while evaluating the effects of vertical excitation. The interaction between the vertical and horizontal response was considered at different seismic levels with a carefully selected ground motion set providing realistic V/H loading for these systems. The results for different systems were obtained for horizontal and vertical ($H + V$), and horizontal only (H) shaking cases focusing on the difference obtained in demand quantities when the vertical motion component was considered. These were presented by expected increase in the demand as well as the corresponding confidence over the whole motion set. The results obtained are summarized as follows:

- Considering vertical excitation along with the horizontal component, the horizontal and vertical accelerations at the crest increase around 10% and 20%, respectively. The horizontal displacements increased by around 5% while the vertical displacement increased between 5% and 10% with no clear trend w.r.t. system size or shaking level.
- Damage was characterized by the width and length of the base crack and the total crack width on the U/S face. The effect of vertical motion on the predicted base crack width was not significant.
- The effect of the vertical motion at the length of the base crack was insignificant. The base crack was obtained 1%–3% longer over the whole motion set considering the vertical components of the motion.
- The total cracking at the upstream face increased considering the vertical ground motion component. The effect was up to 15% and reduced for higher levels of shaking, that is, when the horizontal motions were already significantly high.
- Post-seismic FSS for the base was not affected by the vertical motion, while the corresponding value for the neck was affected significantly at lower levels of ground motion.
- The level of seismic excitation changed the significance of the vertical shaking's effect on behavior. Near cracking or moderate cracking responses were more significantly affected by vertical motion.
- Alternative sets of ground motions were compiled considering different targets in order to evaluate the effect of vertical motions for different motion selection methods. For targets as (horizontal) average spectrum and vertical UHS, little effect on the computed $(V + H)/V$ EDP ratios were observed. The dispersion in the estimates increased considerably for the average spectrum target.

The effect of vertical motions was investigated in this study with the goal of determining the significance of coupling of these motions with horizontal motions in nonlinear THA of concrete gravity dams. The results show vertical components of ground motions should be considered for medium to tall systems (with height > 50 m) at service level or design level earthquakes. The study was conducted using rigid foundation assumptions. The effect of vertical ground motions is increased by the foundation rigidity; correspondingly, the results should be considered as an upper bound for the effect of vertical ground motions for other foundation conditions.

Finally, the ground motion selection in this study was conducted based on real site conditions scanning a large database of motions for complying with state-of-the-art suggestions in determining vertical-horizontal seismic demand. The results show the database regarding the match between both the horizontal and the vertical motions is very limited, particularly for rock site conditions. More response pairs on competent rock foundations are required to quantify V/H ratios for rock sites.

ACKNOWLEDGMENTS

The authors have nothing to report.

DATA AVAILABILITY STATEMENT

The data that support the findings of this study are available from the corresponding author upon reasonable request.

ORCID

Berat Feyza Soysal https://orcid.org/0000-0002-4911-3757
Yalin Arici https://orcid.org/0000-0003-2181-5623
Bekir Özer Ay https://orcid.org/0000-0001-7566-6710

REFERENCES

1. Fenves G, Chopra AK. *Earthquake Analysis and Response of Concrete Gravity Dams*. Earthquake Engineering Research Center; 1984. Report No. UCB/EERC-84/10.

2. Léger P, Leclerc M. Evaluation of earthquake ground motions to predict cracking response of gravity dams. *Eng Struct*. 1996;18(3):227-239. doi:10.1016/0141-0296(95)00146-8
3. Hariri-Ardebili MA, Saouma V. Collapse fragility curves for concrete dams: comprehensive study. *J Struct Eng*. 2016;142(10):04016075. doi:10.1061/(ASCE)ST.1943-541X.0001541
4. Hariri-Ardebili MA, Seyed-Kolbadi SM, Kianoush MR. FEM-based parametric analysis of a typical gravity dam considering input excitation mechanism. *Soil Dyn Earthq Eng*. 2016;84:22-43. doi:10.1016/j.soildyn.2016.01.013
5. Wang G, Wang Y, Lu W, Yan P, Zhou W, Chen M. A general definition of integrated strong motion duration and its effect on seismic demands of concrete gravity dams. *Eng Struct*. 2016;125:481-493. doi:10.1016/j.engstruct.2016.07.033
6. Cundall PA. A computer model for simulating progressive large-scale movements in blocky rock systems. Paper presented at: *Proceedings of The International Symposium on Rock Fracture*; 4–6th October 1971; France.
7. Soysal Albostan BF. *Discrete Element Based Analyses of Structure-Reservoir Problem for Gravity Dams*. PhD thesis. Middle East Technical University; 2021.
8. Fenves G, Chopra AK. Simplified earthquake analysis of concrete gravity dams. *J Struct Eng*. 1987;113(8):1688-1708. doi:10.1061/(ASCE)0733-9445(1987)113:8(1688)
9. Meguro K, Tagel-Din H. Applied element method for structural analysis: theory and application for linear materials. *Struct Eng Earthq Eng*. 2000;647:31-45.
10. Lubliner J, Oliver J, Oller S, Onate E. A plastic-damage model for concrete. *Int J Solids Struct*. 1989;25(3):299-326. doi:10.1016/0020-7683(89)90050-4
11. Maekawa K, Okamura H, Pimanmas A. *Non-linear Mechanics of Reinforced Concrete*. CRC Press; 2003. doi:10.1201/9781482288087
12. Soysal BF, Arici Y, Tuncay K. A modified applied element model for the simulation of plain concrete behaviour. *Mag Concr Res*. 2022;75:325-338. doi:10.1680/jmacr.22.00059
13. Gopalaratnam VS, Shah SP. Softening response of plain concrete in direct tension. *J Am Concr Inst*. 1985;82(3):310-323. doi:10.14359/10338
14. Carpinteri A, Valente S, Ferrara G, Imperato L. Experimental and numerical fracture modelling of a gravity dam. *ACI Symp Publication*. 1992;143:107-122. doi:10.14359/4582
15. Nooru-Mohamed MB. *Mixed-Mode Fracture of Concrete: An Experimental Approach*. PhD thesis. Delft University of Technology; 1992.
16. Wang X, Bathe KJ. Displacement/pressure based mixed finite element formulations for acoustic fluid-structure interaction problems. *Int J Numer Methods Eng*. 1997;40:2001-2017. doi:10.1002/(SICI)1097-0207(19970615)40:11<2001::AID-NME152>3.0.CO;2-W
17. Bathe KJ. *Finite Element Procedures*. Prentice-Hall, Inc; 1996.
18. Sommerfeld A. *Partial Differential Equations in Physics*. Academic Press; 1949. doi:10.1016/b978-0-12-654658-3.x5001-0
19. Bouaanani N, Lu FY. Assessment of potential-based fluid finite elements for seismic analysis of dam-reservoir systems. *Comput Struct*. 2009;87:206-224. doi:10.1016/j.compstruc.2008.10.006
20. Løkke A, Chopra AK. Direct finite element method for nonlinear analysis of semi-unbounded dam-water-foundation rock systems. *Earthq Eng Struct Dyn*. 2017;46(8):1267-1285. doi:10.1002/eqe.2855
21. United States Army Corps of Engineers (USACE). *Roller-Compacted Concrete*. 2000. Report No. EM-1110-2-2006.
22. United States Army Corps of Engineers (USACE). *Time-History Dynamic Analysis of Hydraulic Concrete Structures*. 2003. Report No. EP-1110-2-6051.
23. United States Bureau of Reclamation (USBR). *State-of-Practice for the Nonlinear Analysis of Concrete Dams at the Bureau of Reclamation*. OMB No. 0704-0188. 2006.
24. Catchings RDK, Addo O, Goldman MR, Chan JH, Sickler RR, Criley CJ. *Two-Dimensional Seismic Velocities and Structure Variation at Three British Columbia Hydro and Power Authority (BC Hydro) Dam Sites, Vancouver Island, British Columbia, Canada*. U.S. Geological Survey;2019:125. Open-File Rept. 2019-1015. https://pubs.usgs.gov/of/2019/1015/ofr20191015.pdf
25. Houqun C. Seismic safety analysis of tall concrete dams, investigation and insights on critical challenges. *Earthq Eng Eng Vib*. 2020;19:533-539. doi:10.1007/s11803-020-0578-6
26. Akkar S, Sandıkkaya MA, Ay BÖ. Compatible ground-motion prediction equations for damping scaling factors and vertical-to-horizontal spectral amplitude ratios for the broader Europe region. *Bull Earthq Eng*. 2014;12(1):517-547. doi:10.1007/s10518-013-9537-1
27. Bernier C, Monteiro R, Paultre P. Using the conditional spectrum method for improved fragility assessment of concrete gravity dams in Eastern Canada. *Earthq Spectra*. 2016;32(3):1449-1468. doi:10.1193/072015EQS116M
28. Soysal BF, Ay BÖ, Arici Y. An investigation of the ground motion scaling procedures for the nonlinear seismic analyses of concrete gravity dams. *J Earthq Eng*. 2019;23(6):930-953. doi:10.1080/13632469.2017.1342298
29. Jayaram N, Lin T, Baker JW. A computationally efficient ground-motion selection algorithm for matching a target response spectrum mean and variance. *Earthq Spectra*. 2011;27:797-815. doi:10.1193/1.3608002
30. Ay BÖ, Fox MJ, Sullivan TJ. Technical note: practical challenges facing the selection of conditional spectrum-compatible accelerograms. *J Earthq Eng*. 2017;21(1):169-180. doi:10.1080/13632469.2016.1157527
31. Chakrabarti P, Chopra AK. Hydrodynamic effects in earthquake response of gravity dams. *ASCE J Struct Div*. 1974;100:1211-1224.
32. United States Army Corps of Engineers (USACE). *Seismic Design Provisions for Roller-Compacted Concrete Dams*. 1995. Report No. EP-1110-2-12.

33. Kohrangi M, Bazzurro P, Vamvatsikos D, Spillatura A. Conditional spectrum-based ground motion record selection using average spectral acceleration. *Earthq Eng Struct Dyn*. 2017;46(10):1667-1685.
34. Gülerce Z, Abrahamson NA. Site-specific design spectra for vertical ground motion. *Earthq Spectra*. 2011;27(4):1023-1047.

How to cite this article: Soysal BF, Arici Y, Ay BÖ. The effect of vertical motions on damage accumulation on concrete gravity dams. *Earthquake Engng Struct Dyn*. 2023;52:2619–2638. https://doi.org/10.1002/eqe.3886